Nano-Gold Diggers: Au-Assisted SiO_2-Decomposition and Desorption in Supported Nanocatalysts

Luis K. Ono,[†] Farzad Behafarid,[†] and Beatriz Roldan Cuenya[†,‡,*]

[†]Department of Physics, University of Central Florida, Orlando, Florida 32816, United States, and [‡]Department of Physics, Ruhr University Bochum, 44780 Bochum, Germany

ABSTRACT An investigation of the thermal stability of size-selected Au nanoparticles (NPs) synthesized *via* inverse micelle encapsulation and deposited on SiO_2(4 nm)/Si(100) is presented. The size and mobility of individual Au NPs after annealing at elevated temperatures in ultrahigh vacuum (UHV) was monitored via atomic force microscopy (AFM). An enhanced thermal stability against coarsening and lack of NP mobility was observed up to 1343 K. In addition, a drastic decrease in the average NP height was detected with increasing annealing temperature, which was not accompanied by the sublimation of Au atoms/clusters in UHV. The apparent decrease in the Au NP height observed is assigned to their ability to dig vertical channels in the underlying SiO_2 support. More specifically, a progressive reduction in the thickness of the SiO_2 support underneath and in the immediate vicinity of the NPs was evidenced, leading to NPs partially sinking into the SiO_2 substrate. The complete removal of silicon oxide in small patches was observed to take place around the Au NPs after annealing at 1343 K in UHV. These results reveal a Au-assisted oxygen desorption from the support via reverse oxygen spillover to the NPs.

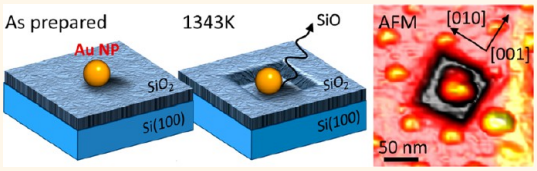

KEYWORDS: Au · nanoparticle · SiO_2 · Si · AFM · atomic force microscopy · XPS · X-ray photoelectron spectroscopy · NP-support interaction

It has been shown that the catalytic properties of small Au nanoparticles (NPs) (<5 nm) can be controlled by modifying their size.[1−7] Additionally, metal−support interactions also affect the activity and selectivity of nanoscale Au catalysts.[8−11] While NP catalysts exhibit many favorable properties, they are prone to drastic structural/morphological changes in response to different thermal and chemical environments.[12−16] The latter include undesired coarsening phenomena leading to reduced surface areas and a consequent decrease in reactivity and change in selectivity.[17−21] Therefore, a thorough understanding of the processes that affect the stability of NP catalysts and when possible, its enhancement via the selection of novel synthesis approaches,[22,23] sample pretreatments,[24] or stabilizing supports,[25−34] is crucial for the application of these systems in an industrial setting.[35,36]

Numerous previous studies described thermally-[22,23,37−40] and chemically-induced[23,24,29,41−44] deactivation processes of NP catalysts involving sintering. Two pathways for NP sintering were generally proposed: (i) Ostwald ripening (OR), in which atom-by-atom diffusion predominantly occurs from small to large clusters,[45−47] and (ii) the diffusion of entire NPs and subsequent coalescence with other NPs.[19−22,38,48] Since the driving force behind coarsening phenomena is to reduce the surface energy of the NPs, the tendency of a NP catalyst to sinter strongly depends on its average size and size distribution.[49−53] Additionally, the interparticle spacing also affects sintering, with widely spaced NPs showing enhanced stability.[23,29]

Nanoparticle-support interactions play a key role in the stabilization of nanoscale systems under environmental conditions, with parameters such as the chemical composition or reducibility of the oxide support[22,23] and its thickness[54] having a strong influence in NP sintering. The present work describes the outstanding stability against sintering of narrowly sized distributed micellar Au NPs homogeneously dispersed over SiO_2(4 nm)/Si(100) substrates upon high temperature thermal treatments in ultrahigh vacuum (UHV). The morphological evolution of individual NPs was monitored *ex situ via*

* Address correspondence to Beatriz.Roldan@rub.de.

Received for review September 9, 2013 and accepted November 1, 2013.

Published online November 01, 2013
10.1021/nn404744b

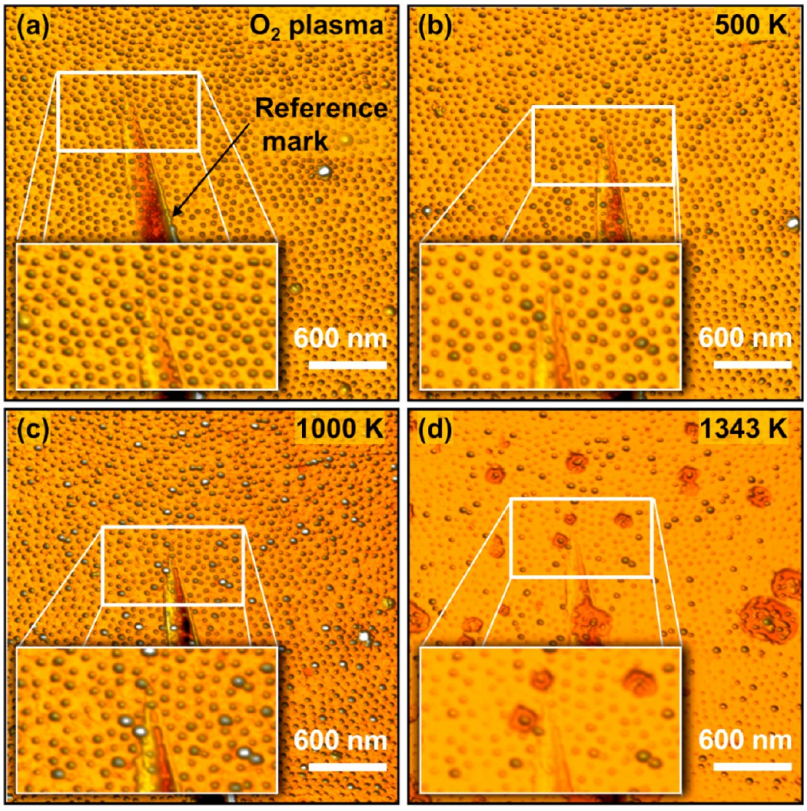

Figure 1. 3000 × 3000 nm^2 AFM images showing the thermal evolution of micelle-synthesized Au NPs supported on SiO_2(∼4 nm)/Si(100). All images were acquired *ex situ* at RT. Image (a) was taken after the removal of the encapsulating ligands by an O_2-plasma at RT, (b) after heating in UHV at 500 K (30 min), (c) after 1000 K (30 min), and (d) after 1343 K (1 min). The inset in each image is a zoomed image of the region marked with white rectangle.

atomic force microscopy (AFM) with the aid of a NP tracking technique based on a substrate marker. For our micelle-synthesized NPs, no NP mobility was detected upon annealing in UHV up to 1343 K. Moreover, low-temperature Au-assisted silicon oxide decomposition was detected, with the gold NPs digging channels in the SiO_2 support. This interesting effect results in the enhanced stability of the NPs against sintering, while a significant fraction of the NP surface area remains accessible to reactants. The latter makes them promising materials for catalysis and sensing applications.

RESULTS AND DISCUSSION

Figure 1 shows AFM images of a Au NP/SiO_2/Si(100) sample acquired at room temperature (RT) after the following treatments: (a) O_2-plasma (ligand removal), (b) heating in UHV at 500 K, (c) 1000 K, and (d) at 1343 K. A reference mark at the bottom of each image allows us to investigate the same sample region *ex situ* after the different *in situ* treatments. Table 1 contains information on the average NP height and interparticle distances of our sample after the annealing treatments. The corresponding histograms are shown in Figure 2 and Supporting Information, Figure 1. After O_2-plasma exposure, a uniform arrangement of monodispersed Au NPs (homogeneous image brightness and associated NP height) is observed (Figure 1a). Annealing at 500 K leads to an increase in the number of bright spots in the images, revealing the gradual loss of the regularity in the NP height distribution (Figure 1b). Subsequent annealing at 1000 K (Figure 1c) leads to a more pronounced height contrast, indicating the existence of a wider size distribution. The images in Figure 1 and related interparticle distance histograms (Supporting Information, Figure 1) indicate the lack of mobility of our Au NPs, ruling out possible NP coarsening phenomena *via* diffusion-coalescence. In addition, no increase in the average NP height was observed upon heating for the majority of the NPs, Figure 2, but a progressive decrease from 4.6 ± 1.1 nm (as prepared ligand-free NPs), to 2.8 ± 1.3 nm after heating at 500 K, 2.0 ± 1.3 nm after 1000 K, and 2.1 ± 1.6 nm after 1343 K. Despite the fact that the majority of the NPs in our

TABLE 1. Summary of the Height and Interparticle Distance Distributions of Micellar Au NPs Supported on SiO_2(∼4 nm)/Si(100) after O_2-Plasma and Subsequent Thermal Treatments in UHV

treatments	height (nm)	interparticle distance (nm)
O_2-plasma	4.6 ± 1.1	76 ± 19
500 K (30 min)	2.8 ± 1.3	72 ± 16
1000 K (30 min)	2.0 ± 1.3	76 ± 20
1343 K (1 min)	2.1 ± 1.6	74 ± 21

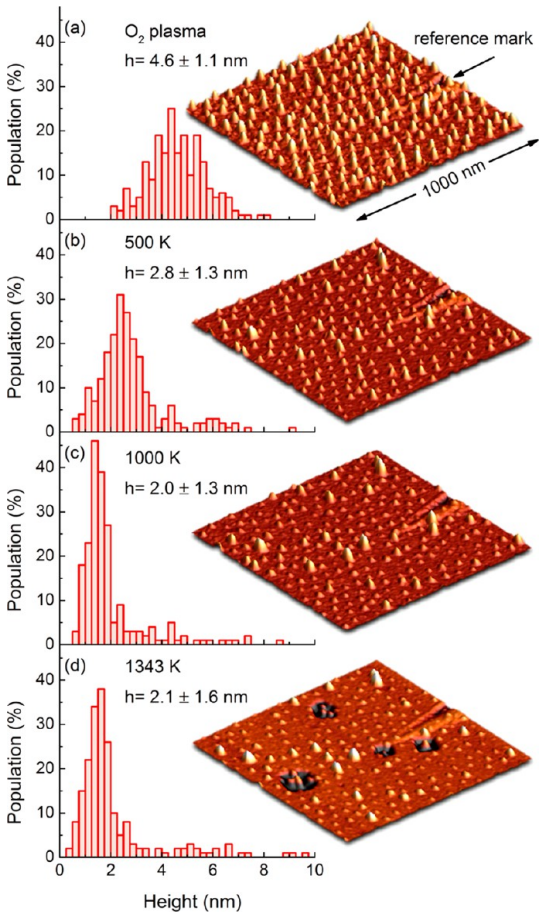

Figure 2. NP height histograms based on AFM images of Au NPs on SiO_2(~4 nm)/Si(100). The data displayed were obtained after (a) an O_2-plasma treatment at RT and subsequent heating in UHV at (b) 500 K, (c) 1000 K, and (d) 1343 K (see Figure 1 for details).

sample become smaller with increasing annealing temperature, a small fraction of large NPs is observed above 500 K. Considering the lack of NP mobility, such observation might be explained based on Ostwald ripening processes[49,58] in which the growth of large NPs is mediated by the donation of atoms from the surrounding smaller NPs.

While Ostwald ripening might explain the growth of a small number of large particles, it does not explain the significant height reduction observed for the majority of the NPs. A part of this decrease could be explained based on the reduction of Au oxide species formed during the O_2-plasma treatment. Considering the density of Au_2O_3 of 11 g/cm^3,[55] and that of metallic Au of 19.3 g/cm^3, the final NP volume after the complete reduction of the gold oxide species would be ~0.6 of the initial volume. Nevertheless, such reduction in volume would translate to only ~17% reduction in NP height, which is insignificant as compared to the strong decrease in size observed.

Another possibility that should be taken into consideration is the formation of Au silicide species. It has been shown that even at relatively low temperatures, metals such as Au could form silicides when deposited on bare silicon substrates.[56−58] However, such behavior is not expected when the Au films or nanoparticles are separated from the silicon interface by relatively thick (~4 nm in the present case) SiO_2 films. We have ruled out such a possibility on the basis of the lack of gold silicide features in our Au-4f XPS spectra. The formation of gold silicide has been shown to shift the Au-4f peaks to higher binding energies, for example, from ~84.1 eV expected for bulk gold up to ~85.1 eV in a study conducted on a thick Au overlayer deposited on a bare silicon substrate.[59] In our example, the Au-4f spectra could be fitted with only one component, demonstrating the chemical homogeneity of the NPs, and the binding energies measured (Au-4$f_{7/2}$ ~84.6 eV) are significantly lower than those characteristic of Au silicide. It should be noted that the smaller shifts observed here in the Au-4f core levels are typical of small NPs and are assigned to size effects.[60,61] Accordingly, if Au silicide species were present in our samples, it should be in minute amounts well below our detection limit, and these species are not likely to play any significant role in the NP stability or drastic height reduction observed.

An additional plausible explanation for the overall particle height reduction is the loss of Au atoms through a sublimation process. In contrast to a melting temperature of ~1337 K[62] for bulk Au, a lower melting temperature of ~1150 K has been reported for ~5 nm Au NPs.[62−64] To investigate this possibility, XPS measurements were conducted after the different chemical/thermal treatments (Figure 3). For a sample treated *in situ*, the ratio of Au-4f/Si-2p areas remains nearly constant after all treatments up to 1343 K (~0.24, see Supporting Information, Table 1), indicating the lack of gold sublimation or loss in UHV (Figure 3a). However, a different behavior is observed when an analogously treated sample is exposed to air after each *in situ* treatment, as was the case of the sample used here for AFM analysis. In the latter case, the gold oxide species present in the as-prepared sample after atomic oxygen exposure disappear after air exposure for 20h at room temperature, Figure 3b. A similar finding was reported for the decomposition of oxidized bulk gold samples by Tsai et al.,[65] and air moisture was shown to be involved in this phenomenon, since no Au reduction was observed in dry CO_2 after 6 days.[66] Nevertheless, it should be noted that our XPS data did not reveal the decomposition of Au_2O_3 into metallic Au upon air exposure, but its disappearance and consequent loss of gold. In fact, while the XPS area under the Au metallic peak remains similar before and after air exposure, the oxide component vanishes entirely. This finding indicates that the mechanism underlying the reduction of Au_2O_3 at room temperature in air involves the loss (volatilization) of Au oxide species, and not its decomposition to metallic gold

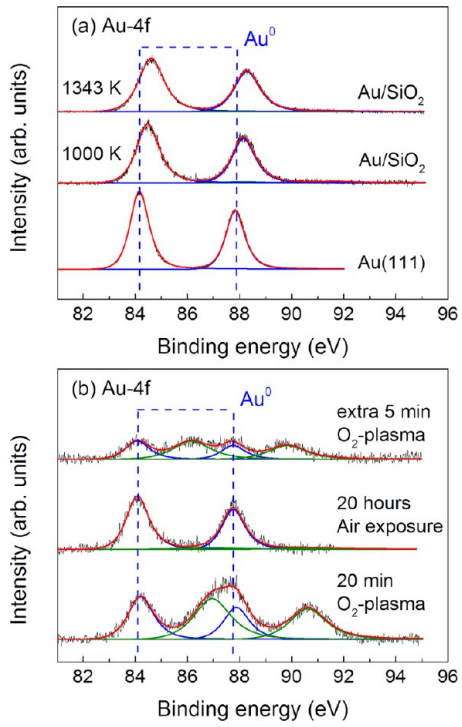

Figure 3. Au-4f XPS data of Au NPs on SiO_2(~4 nm)/Si(100) (a) cleaned with an O_2-plasma and acquired after annealing at different temperatures, (b) XPS spectra acquired directly after an O_2-plasma treatment, after a subsequent 20 h exposure to air at atmospheric pressure, and after a 5 min additional O_2-plasma treatment. The Au-4f XPS spectrum of Au(111) is shown in panel (a) as reference.

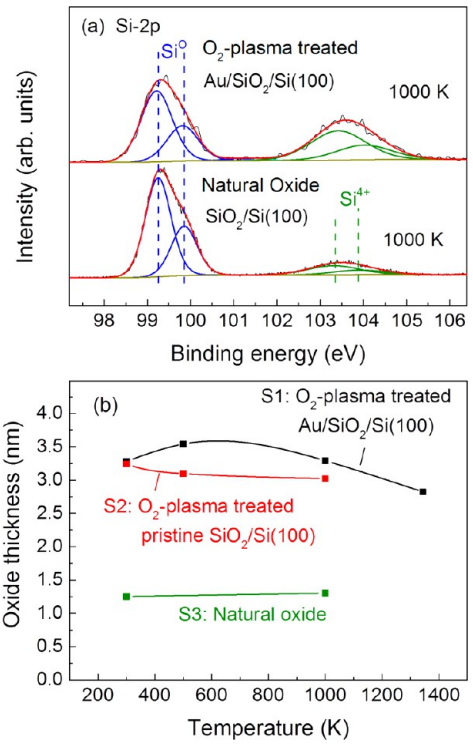

Figure 4. (a) Si-2p XPS data of a silicon substrate with a thin film of natural oxide as well as a another sample treated with an O_2-plasma, and (b) the oxide thickness obtained from XPS analysis of the Au NP SiO_2/Si(100) samples and a pristine SiO_2/Si(100) substrate measured after O_2-plasma treatment and annealing at different temperatures. Data from a natively oxidized silicon sample are also included for reference.

accompanied by oxygen desorption.[65] To rule out the signal damping due to carbon deposition during air exposure, the same sample was additionally cleaned by an O_2-plasma, but the Au-4f intensity did not recover its initial value (Figure 3b). Therefore, we can conclude that the strong decrease in NP height observed via AFM for the sample exposed to air from RT to 500 K can be at least partially assigned to the loss of the Au_2O_3 species. Nevertheless, a different phenomenon must underlie the further decrease in AFM NP height observed above 500 K, when no (or only a small fraction) Au_2O_3 species were present in our sample. Since for NPs within this size range AFM measurements do not provide reliable information on the NPs lateral size, the alternative possibility of NP flattening as being responsible for the observed decrease in the NP height was considered. Nevertheless, following the Beer–Lambert attenuation law, such NP flattening should increase the Au-4f/Si-2p ratio due to the smaller travel length of Au photoelectrons inside the NPs upon the 3D (spherical) to 2D (flat) NP shape change, which was not observed here.

A final possibility to explain the apparent reduction in gold NP size upon annealing above 500 K is their incorporation into the SiO_2 support ("nano-Au diggers"), that is, their ability to dig channels into the underlying SiO_2 substrate by contributing to its decomposition and subsequent desorption. The loss of SiO_2 patches around the NPs is in fact observed in Figure 1d. This phenomenon could explain the enhanced stability and the lack of NP mobility observed by AFM. To explore this hypothesis and to gain further insight into the role of the Au NPs in this SiO_2 decomposition process ($T \leq 1343$ K), XPS data of the Si-2p core level region were acquired after the different treatments. Figure 4a shows XPS data of a pristine silicon substrate (NP-free) with a thin layer of natural oxide and also a ligand-free Au NP/SiO_2 sample after annealing at 1000 K. The contribution of the Si^{4+} peak (at ~103.3 eV) is much larger for the Au NP/SiO_2 sample than for the clean natively oxidized SiO_2/Si(001) substrate due to the O_2-plasma treatment undergone by the former. Considering the inelastic mean free path (IMFP) of photoelectrons, an estimation of the oxide layer thickness was made based on the Si^0, Si^{x+}, and Si^{4+} XPS intensities. The details on the method used for the calculation of the oxide thickness are provided in the supplementary documents. Here, we need to mention that the Si^{4+}/Si^0 ratio obtained by XPS is not affected by the presence of the Au NPs on the support surface due to their low coverage and to the fact that Si^0 and Si^{4+} photoelectrons have similar inelastic mean free paths inside the Au NPs, and therefore, such signals will be

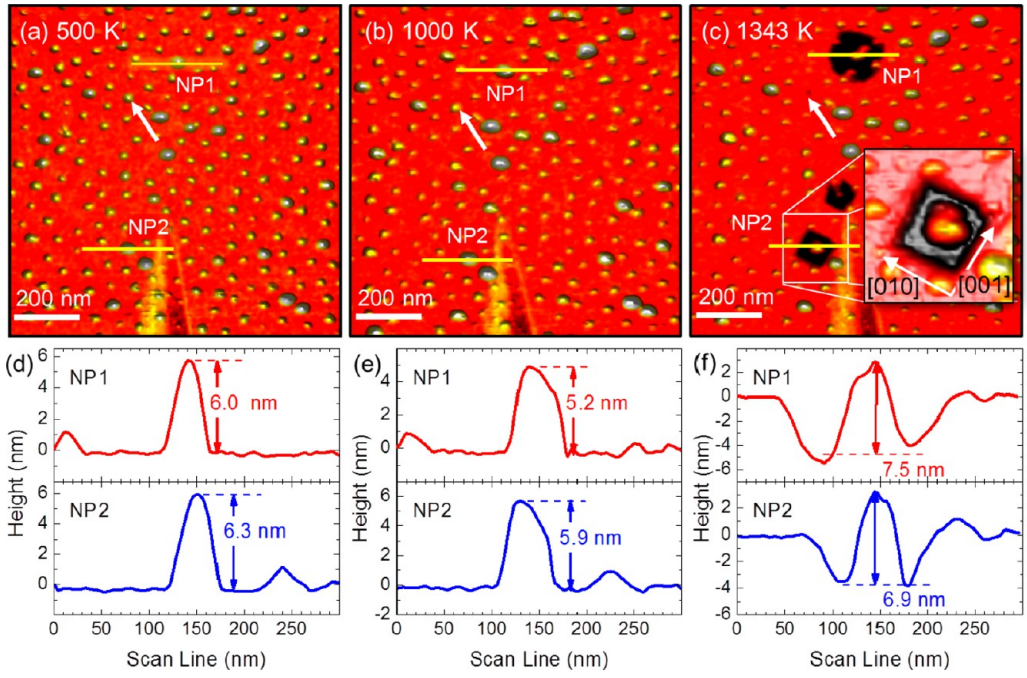

Figure 5. AFM images of Au NPs on SiO_2(~4 nm)/Si(100) acquired after annealing in UHV at (a) 500 K, (b) 1000 K, and (c) 1343 K (see Figure 1 for details). A line profile analysis of the height of several individual Au NPs is also shown.

affected in the same manner by the presence of the Au overlayer.

The summary of the oxide thicknesses obtained after the different thermal treatments is displayed in Figure 4b for three different samples: (i) sample S1, Au NP/SiO_2/Si(100) pretreated with an O_2-plasma, (ii) sample S2, a pristine silicon substrate treated with an O_2-plasma similarly to S1, and (iii) sample S3, a pristine Si(100) substrate with a thin native oxide overlayer and no plasma treatment. A drastic difference in the oxide thicknesses could be observed for the two samples that were treated with the O_2-plasma (S1,S2) as compared to the natively oxidized one (S3). Nevertheless, although directly after the plasma treatment samples S1 and S2 have similar oxide thicknesses, after the first annealing at 500 K the oxide thickness increases for S1, while it decreases slightly for S2. This observation hints toward an oxygen spillover effect from the Au NPs present in S1 to SiO_2, which results in excess oxygen inside our amorphous SiO_2 film. The mild annealing at 500K might allow the diffusion of interstitial oxygen trapped in the oxide layer to the underlying Si(100), resulting in the further growth of the oxide layer. As can be seen from the data of S2, such phenomenon does not occur in the absence of the Au NPs. Our findings are in agreement with a previous study by Campbell,[67] showing that when bimetallic surfaces are oxidized, the dissociation temperature of the most stable oxides upon heating in UHV is generally reduced in the presence of a metal with a less stable oxide.

By annealing the samples at higher temperature (*i.e.*, 1000 K), a decrease in the oxide thickness is observed for S1, which is explained based on the decomposition of SiO_2. The same phenomenon is not observed for the NP-free samples (S2, S3), suggesting that the Au NPs might act as catalysts to reduce the underlying oxide support at relatively mild temperatures for this system. Such reduction should occur at the NP-support interface, leading to the removal of the SiO_2 support underneath the NPs, with the NPs becoming partially embedded into the oxide layer. At the highest annealing temperature of this study (1343 K), the removal of big patches of silicon dioxide is evident around some of the Au NPs, Figure 1d. Here we have to keep in mind the AFM tip convolution effect resulting in an overestimation of the NP diameter. Such effect might mask the formation of recessions and areas of missing oxide around the NPs at lower temperatures, only becoming visible when they extend far beyond the NP perimeter. Therefore, at low temperature, the only indication of the Au NPs sinking into the support is the apparent decrease in their height.

Figure 5 features high resolution AFM images from a selected sample region where the desorption of oxide patches around the Au NPs was observed at 1343 K. As expected, the height profiles from the NPs surrounded by dark rings (missing silicon oxide) reveal a rather similar NP height when comparing 500 K and 1343 K data, confirming that no significant loss of Au occurred under the experimental conditions. Therefore, the apparent decrease in height of these NPs at intermediate temperatures could be accounted for by considering the changes in the SiO_2 thickness underneath the NPs and the incorrect assumption of the SiO_2 base background in the histograms of Figure 2.

The major morphological changes observed for the micelle-synthesized Au NPs supported on SiO_2/Si are schematically depicted in Figure 6. The NP in the as

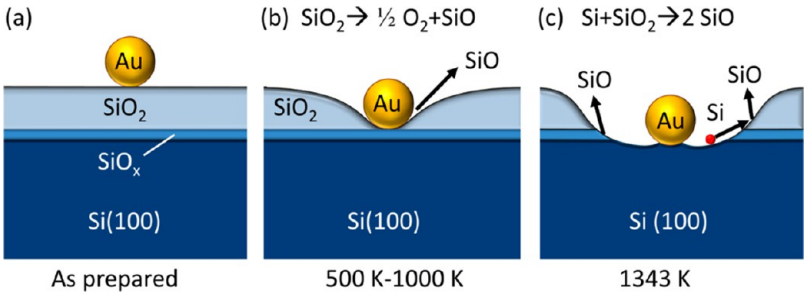

Figure 6. Schematic representation of the morphological changes of individual Au NPs supported on SiO_2/Si(100) upon annealing treatments in UHV. Volatile SiO species escape the sample after a catalytic reduction of the SiO_2 support mediated by the Au NPs.

prepared sample digs a channel into the silicon oxide after each thermal treatment due to the progressive desorption of volatile SiO compounds. As soon as the NP removes the underlying oxide layer entirely and digs a hole into the Si(100) underneath, Figure 6c, the growth of the depression around the NPs could be continued without any further assistance from the NP. In most reducible oxide supports such as TiO_2, the oxide decomposition occurs via desorption of oxygen atoms and consequent inward diffusion of remained cations into the interstitial sites in the bulk.[68,69] However, in case of SiO_2, the oxide decomposition mainly occurs through the desorption of volatile SiO, and not only that of oxygen. Since the SiO_x layer is trapped at the interface between the bulk Si(100) support and the SiO_2 overlayer which is much more stable, it cannot escape into vacuum as long as the SiO_2 layer is intact.[70] However, after the Au NPs dig a channel into the oxide layer and expose the underlying bulk Si(100), the oxide decomposition might accelerate significantly. At that point, silicon atoms could diffuse on the exposed bare silicon patch and reach the oxide layer at the edge of the hole to form volatile SiO and escape into vacuum. As could be seen in the inset of Figure 5c, the square shape of the recessed area around the Au NP demonstrates that the desorption of SiO occurs predominantly along steps in the (010) and (001) directions of the Si(100) substrate.

Summarizing, surprisingly strong NP/support interactions, leading the fast and relatively low-temperature decomposition of SiO_2 species were discovered for micellar Au NPs supported on thin amorphous O_2-plasma-grown SiO_2 films. As a result of such interaction, the Au NPs dig themselves into the SiO_2 support and became stabilized against sintering. Since even at 1343 K the NPs do not become completely embedded into the SiO_2 support, this thermally stable system might be suitable for industrial applications in the fields of sensing and catalysis.

CONCLUSION

The thermal stability and mobility of size-selected micellar Au NPs supported on SiO_2/Si(100) was studied by AFM. Our microscopy data evidenced lack of NP mobility up to 1343 K but an overall apparent decrease in the NP height with increasing annealing temperature which, according to XPS, could not be explained in terms of Au sublimation. The drastic morphological changes observed upon heating at relatively low temperature (<1000 K) can only be understood if the desorption of oxygen and decomposition of SiO_2 underneath the NPs and at their perimeter is considered, leading to NPs sinking into the thin SiO_2 substrate. The latter effect might also explain the superior thermal stability of the NPs against sintering, since they become trapped into substrate channels that they create themselves by assisting the decomposition of SiO_2 species and subsequent desorption of SiO and O_2. The preferential removal of oxide patches, although initially nucleated by NPs, could subsequently grow further on its own with increasing annealing temperature or time. This material system is expected to be of interest for high temperature applications where sintering-resistant oxide-supported metal NPs are required.

EXPERIMENTAL SECTION

Hexagonally ordered arrays of Au NPs were synthesized by an inverse micelle encapsulation technique.[1,29,41,53,71] Reverse micelles formed from the dissolution of polystyrene-block-poly(2-vynilpyridine) [PS(*x*)-b-P2VP(*y*), Polymer Source Inc.] in toluene are subsequently loaded with $HAuCl_4 \cdot 3H_2O$. The NP size is tuned by changing the molecular weight of the polymer core (P2VP) and by tuning the gold salt to P2VP ratio. The molecular weight of the polymer tail (PS) determines the interparticle distance. The polymer used for the synthesis was PS(81000)-b-P2VP(14200), with a metal salt/P2VP concentration ratio of 0.2. Amorphous naturally oxidized SiO_2 thin films on Si(100) wafers were used as substrates. A reference mark was made on the substrate surface prior to NP deposition with a diamond scribe. Substrate dip-coating into the gold polymeric solution at a speed of 10 mm/min resulted in a monolayer-thick film of nearly monodispersed micelles containing Au NPs.

The *ex situ* prepared samples were transferred into a UHV system for the removal of the encapsulating ligands via an O_2 plasma treatment ($P_{O_2} = 5.5 \times 10^{-5}$ mbar for 100 min) at room temperature (RT). The thermal stability of the NPs was monitored *ex situ* at RT via AFM (Digital Instruments Nanoscope III,

tapping mode) after *in situ* (UHV) annealing at 500 K (for 30 min), 1000 K (for 30 min), and 1343 K (for 1 min). The AFM tip was positioned close to the reference mark made on the SiO_2/Si(100) substrate with the aid of an optical microscope, and silicon nitride AFM tips with an end radius below 10 nm were used for scanning. The cantilevers employed have resonant frequencies in the range of 300−330 kHz with spring constants of about 42 N/m. A typical scan rate of 1 Hz was used to acquire the images, and the tip−sample interaction was minimized to avoid tip-induced distortions in the NP shape and/or NP arrangement during scanning. Because of tip-convolution effects, the NP height (and not the diameter) was used as representative size parameter. Our NP tracking method allows the observation of the behavior of individual NPs in a large area (3000 nm × 3000 nm) and and a direct comparison of the morphological changes of a large number of individual NPs within the ensemble. X-ray photoelectron spectroscopy (XPS) was used to monitor changes in the chemical composition of the NPs and SiO_2/Si(100) support after the O_2-plasma treatments and UHV annealing. No Cl-2p signal was detected by XPS after O_2-plasma treatment.

Conflict of Interest: The authors declare no competing financial interest.

Supporting Information Available: Additional AFM and XPS data analysis. This material is available free of charge *via* the Internet at http://pubs.acs.org.

Acknowledgment. This work was supported by the US National Science Foundation, NSF-CHEM-1213182. Partial financial support by the Cluster of Excellence RESOLV (DFG. EXC-1069) at the Ruhr-University Bochum is also acknowledged.

REFERENCES AND NOTES

1. Roldan Cuenya, B. Synthesis and Catalytic Properties of Metal Nanoparticles: Size, Shape, Support, Composition, and Oxidation State Effects. *Thin Solid Films* **2010**, *518*, 3127–3150.
2. Green, I. X.; Tang, W. J.; Neurock, M.; Yates, J. T. Spectroscopic Observation of Dual Catalytic Sites During Oxidation of CO on a Au/TiO_2 Catalyst. *Science* **2011**, *333*, 736–739.
3. Laoufi, I.; Saint-Lager, M. C.; Lazzari, R.; Jupille, J.; Robach, O.; Garaudee, S.; Cabailh, G.; Dolle, P.; Cruguel, H.; Bailly, A. Size and Catalytic Activity of Supported Gold Nanoparticles: An *in Operando* Study during CO Oxidation. *J. Phys. Chem. C* **2011**, *115*, 4673–4679.
4. Herzing, A. A.; Kiely, C. J.; Carley, A. F.; Landon, P.; Hutchings, G. J. Identification of Active Gold Nanoclusters on Iron Oxide Supports for CO Oxidation. *Science* **2008**, *321*, 1331–1335.
5. Overbury, S. H.; Schwartz, V.; Mullim, D. R.; Yan, W. F.; Dai, S. Evaluation of the Au Size Effect: CO Oxidation Catalyzed by Au/TiO_2. *J. Catal.* **2006**, *241*, 56–65.
6. Hutchings, G. J.; Haruta, M. A Golden Age of Catalysis: A Perspective. *Appl. Catal., A* **2005**, *291*, 2–5.
7. Valden, M.; Lai, X.; Goodman, D. W. Onset of Catalytic Activity of Gold Clusters on Titania with the Appearance of Nonmetallic Properties. *Science* **1998**, *281*, 1647–1650.
8. Rodriguez, J. A.; Illas, F. Activation of Noble Metals on Metal-Carbide Surfaces: Novel Catalysts for CO Oxidation, Desulfurization and Hydrogenation Reactions. *Phys. Chem. Chem. Phys.* **2012**, *14*, 427–438.
9. Campbell, C. T.; Sharp, J. C.; Yao, Y. X.; Karp, E. M.; Silbaugh, T. L. Insights into Catalysis by Gold Nanoparticles and Their Support Effects through Surface Science Studies of Model Catalysts. *Faraday Discuss.* **2011**, *152*, 227–239.
10. Janssens, T. V. W.; Clausen, B. S.; Hvolbaek, B.; Falsig, H.; Christensen, C. H.; Bligaard, T.; Norskov, J. K. Insights into the Reactivity of Supported Au Nanoparticles: Combining Theory and Experiments. *Top. Catal.* **2007**, *44*, 15–26.
11. Haruta, M. Size- and Support-Dependency in the Catalysis of Gold. *Catal. Today* **1997**, *36*, 153–166.
12. Smith, D. J.; Petfordlong, A. K.; Wallenberg, L. R.; Bovin, J. O. Dynamic Atomic-Level Rearrangements in Small Gold Particles. *Science* **1986**, *233*, 872–875.
13. Ajayan, P. M.; Marks, L. D. Evidence for Sinking of Small Particles into Substrates and Implications for Heterogeneous Catalysis. *Nature* **1989**, *338*, 139–141.
14. Helveg, S.; Hansen, P. L. Atomic-Scale Studies of Metallic Nanocluster Catalysts by *in situ* High-Resolution Transmission Electron Microscopy. *Catal. Today* **2006**, *111*, 68–73.
15. Min, B. K.; Alemozafar, A. R.; Biener, M. M.; Biener, J.; Friend, C. M. Reaction of Au(111) with Sulfur and Oxygen: Scanning Tunneling Microscopic Study. *Top. Catal.* **2005**, *36*, 77–90.
16. Somorjai, G. A. New Model Catalysts (Platinum Nanoparticles) and New Techniques (SFG and STM) for Studies of Reaction Intermediates and Surface Restructuring at High Pressures During Catalytic Reactions. *Appl. Surf. Sci.* **1997**, *121*, 1–19.
17. Paredis, K.; Ono, L. K.; Behafarid, F.; Zhang, Z. F.; Yang, J. C.; Frenkel, A. I.; Roldan Cuenya, B. Evolution of the Structure and Chemical State of Pd Nanoparticles during the *in Situ* Catalytic Reduction of NO with H_2. *J. Am. Chem. Soc.* **2011**, *133*, 13455–13464.
18. Paredis, K.; Ono, L. K.; Mostafa, S.; Li, L.; Zhang, Z. F.; Yang, J. C.; Barrio, L.; Frenkel, A. I.; Roldan Cuenya, B. Structure, Chemical Composition, and Reactivity Correlations during the *in Situ* Oxidation of 2-Propanol. *J. Am. Chem. Soc.* **2011**, *133*, 6728–6735.
19. Wanner, M.; Werner, R.; Gerthsen, D. Dynamics of Gold Clusters on Amorphous Carbon Films Induced by Annealing in a Transmission Electron Microscope. *Surf. Sci.* **2006**, *600*, 632–640.
20. Akita, T.; Lu, P.; Ichikawa, S.; Tanaka, K.; Haruta, M. Analytical TEM Study on the Dispersion of Au Nanoparticles in Au/TiO_2 Catalyst Prepared under Various Temperatures. *Surf. Interface Anal.* **2001**, *31*, 73–78.
21. Mohamed, M. B.; Wang, Z. L.; El-Sayed, M. A. Temperature-Dependent Size-Controlled Nucleation and Growth of Gold Nanoclusters. *J. Phys. Chem. A* **1999**, *103*, 10255–10259.
22. Behafarid, F.; Roldan Cuenya, B. Coarsening Phenomena of Metal Nanoparticles and the Influence of the Support Pre-Treatment: Pt/TiO_2(110). *Surf. Sci.* **2012**, *606*, 908–918.
23. Behafarid, F.; Roldan Cuenya, B. Towards the Understanding of Sintering Phenomena at the Nanoscale: Geometric and Environmental Effects. *Top. Catal.* **2013**, *56*, 1542–1559.
24. Matos, J.; Ono, L. K.; Behafarid, F.; Croy, J. R.; Mostafa, S.; DeLaRiva, A. T.; Datye, A. K.; Frenkel, A. I.; Roldan Cuenya, B. *In situ* Coarsening Study of Inverse Micelle-Prepared Pt Nanoparticles Supported on γ-Al_2O_3: Pretreatment and Environmental Effects. *Phys. Chem. Chem. Phys.* **2012**, *14*, 11457–11467.
25. Zschech, D.; Kim, D. H.; Milenin, A. P.; Hopfe, S.; Scholz, R.; Goring, P.; Hillebrand, R.; Senz, S.; Hawker, C. J.; Russell, T. P.; et al. High-Temperature Resistant, Ordered Gold Nanoparticle Arrays. *Nanotechnology* **2006**, *17*, 2122–2126.
26. Bore, M. T.; Pham, H. N.; Ward, T. L.; Datye, A. K. Role of Pore Curvature on the Thermal Stability of Gold Nanoparticles in Mesoporous Silica. *Chem. Commun.* **2004**, 2620–2621.
27. Gabaldon, J. P.; Bore, M. T.; Datye, A. K. Mesoporous Silica Supports for Improved Thermal Stability in Supported Au Catalysts. *Top. Catal.* **2007**, *44*, 253–262.
28. Tan, B. J. Y.; Sow, C. H.; Koh, T. S.; Chin, K. C.; Wee, A. T. S.; Ong, C. K. Fabrication of Size-Tunable Gold Nanoparticles Array with Nanosphere Lithography, Reactive Ion Etching, and Thermal Annealing. *J. Phys. Chem. B* **2005**, *109*, 11100–11109.
29. Ono, L. K.; Roldan Cuenya, B. Effect of Interparticle Interaction on the Low Temperature Oxidation of CO Over Size-Selected Au Nanocatalysts Supported on Ultrathin TiC Films. *Catal. Lett.* **2007**, *113*, 86–94.
30. Min, B. K.; Wallace, W. T.; Goodman, D. W. Synthesis of a Sinter-Resistant, Mixed-Oxide Support for an Nanoclusters. *J. Phys. Chem. B* **2004**, *108*, 14609–14615.
31. Yan, W. F.; Mahurin, S. M.; Pan, Z. W.; Overbury, S. H.; Dai, S. Ultrastable Au Nanocatalyst Supported on Surface-Modified TiO_2 Nanocrystals. *J. Am. Chem. Soc.* **2005**, *127*, 10480–10481.

32. Qian, K.; Huang, W. X.; Jiang, Z. Q.; Sun, H. X. Anchoring Highly Active Gold Nanoparticles on SiO_2 by CoO_x Additive. *J. Catal.* **2007**, *248*, 137–141.
33. Liu, Z. P.; Jenkins, S. J.; King, D. A. Role of Nanostructured Dual-Oxide Supports in Enhanced Catalytic Activity: Theory of CO Oxidation Over $Au/IrO_2/TiO_2$. *Phys. Rev. Lett.* **2004**, *93*, 156102.
34. Akita, T.; Okumura, M.; Tanaka, K.; Tsubota, S.; Haruta, M. Analytical TEM Observation of Au and Ir Deposited on Rutile TiO_2. *J. Electron Microsc.* **2003**, *52*, 119–124.
35. Bartholomew, C. H. Mechanisms of Catalyst Deactivation. *Appl. Catal., A* **2001**, *212*, 17–60.
36. Sinha, A. K.; Seelan, S.; Tsubota, S.; Haruta, M. Catalysis by Gold Nanoparticles: Epoxidation of Propene. *Top. Catal.* **2004**, *29*, 95–102.
37. Mitchell, C. E. J.; Howard, A.; Carney, M.; Egdell, R. G. Direct Observation of Behaviour of Au Nanoclusters on TiO_2(110) at Elevated Temperatures. *Surf. Sci.* **2001**, *490*, 196–210.
38. Kolmakov, A.; Goodman, D. W. *In Situ* Scanning Tunneling Microscopy of Oxide-Supported Metal Clusters: Nucleation, Growth, and Thermal Evolution of Individual Particles. *Chem. Rec.* **2002**, *2*, 446–457.
39. Heemeier, M.; Stempel, S.; Shaikhutdinov, S. K.; Libuda, J.; Baumer, M.; Oldman, R. J.; Jackson, S. D.; Freund, H. J. On the Thermal Stability of Metal Particles Supported on a Thin Alumina Film. *Surf. Sci.* **2003**, *523*, 103–110.
40. Matthey, D.; Wang, J. G.; Wendt, S.; Matthiesen, J.; Schaub, R.; Laegsgaard, E.; Hammer, B.; Besenbacher, F. Enhanced Bonding of Gold Nanoparticles on Oxidized TiO_2(110). *Science* **2007**, *315*, 1692–1696.
41. Ono, L. K.; Sudfeld, D.; Roldan Cuenya, B. *In Situ* Gas-Phase Catalytic Properties of TiC-Supported Size-Selected Gold Nanoparticles Synthesized by Diblock Copolymer Encapsulation. *Surf. Sci.* **2006**, *600*, 5041–5050.
42. Sehested, J.; Gelten, J. A. P.; Helveg, S. Sintering of Nickel Catalysts: Effects of Time, Atmosphere, Temperature, Nickel-Carrier Interactions, and Dopants. *Appl. Catal., A* **2006**, *309*, 237–246.
43. Laurin, M.; Johanek, V.; Grant, A. W.; Kasemo, B.; Libuda, J.; Freund, H. J. Local Reaction Rates and Surface Diffusion on Nanolithographically Prepared Model Catalysts: Experiments and Simulations. *J. Chem. Phys.* **2005**, *122*, 084713.
44. Zhou, J.; Kang, Y. C.; Ma, S.; Chen, D. A. Adsorbate-Induced Dissociation of Metal Clusters: TiO_2 (110)-Supported Cu and Ni Clusters Exposed to Oxygen Gas. *Surf. Sci.* **2004**, *562*, 113–127.
45. Lu, J. L.; Gao, H. J.; Shaikhutdinov, S.; Freund, H. J. Gold Supported on Well-Ordered Ceria Films: Nucleation, Growth and Morphology in CO Oxidation Reaction. *Catal. Lett.* **2007**, *114*, 8–16.
46. Lai, X. F.; Goodman, D. W. Structure-Reactivity Correlations for Oxide-Supported Metal Catalysts: New Perspectives from STM. *J. Mol. Catal. A* **2000**, *162*, 33–50.
47. Starr, D. E.; Shaikhutdinov, S. K.; Freund, H. J. Gold Supported on Oxide Surfaces: Environmental Effects as Studied by STM. *Top. Catal.* **2005**, *36*, 33–41.
48. Bowker, M. Surface science—The Going Rate for Catalysts. *Nat. Mater.* **2002**, *1*, 205–206.
49. Campbell, C. T.; Parker, S. C.; Starr, D. E. The Effect of Size-Dependent Nanoparticle Energetics on Catalyst Sintering. *Science* **2002**, *298*, 811–814.
50. Parker, S. C.; Campbell, C. T. Reactivity and Sintering Kinetics of Au/TiO_2(110) Model Catalysts: Particle Size Effects. *Top. Catal.* **2007**, *44*, 3–13.
51. Ajayan, P. M.; Marks, L. D. Experimental-Evidence for Quasimelting in Small Particles. *Phys. Rev. Lett.* **1989**, *63*, 279–282.
52. Ajayan, P. M.; Iijima, S. Wetting and De-wetting Transitions of Small Metal Particles on Substrates under Electron-Irradiation. *J. Colloid Interface Sci.* **1991**, *147*, 281–285.
53. Kastle, G.; Boyen, H. G.; Weigl, F.; Lengl, G.; Herzog, T.; Ziemann, P.; Riethmuller, S.; Mayer, O.; Hartmann, C.; Spatz, J. P.; *et al.* Micellar Nanoreactors—Preparation and Characterization of Hexagonally Ordered Arrays of Metallic Nanodots. *Adv. Funct. Mater.* **2003**, *13*, 853–861.
54. Santra, A. K.; Goodman, D. W. Oxide-Supported Metal Clusters: Models for Heterogeneous Catalysts. *J. Phys. Condens. Matter* **2003**, *15*, R31–R62.
55. King, D. E. Oxidation of Gold by Ultraviolet Light and Ozone at 25 °C. *J. Vac. Sci. Technol., A* **1995**, *13*, 1247–1253.
56. Green, A. K.; Bauer, E. Formation, Structure, and Orientation of Gold Silicide on Gold Surfaces. *J. Appl. Phys.* **1976**, *47*, 1284–1291.
57. Mundschau, M.; Bauer, E.; Telieps, W.; Święch, W. Initial Epitaxial Growth of Copper Silicide on Si{111} Studied by Low-Energy Electron Microscopy and Photoemission Electron Microscopy. *J. Appl. Phys.* **1989**, *65*, 4747–4752.
58. Chambers, S.; Anderson, S.; Chen, H.; Weaver, J. High-Temperature Nucleation and Silicide Formation at the Co/Si(111)-7 × 7 Interface: A Structural Investigation. *Phys. Rev. B* **1986**, *34*, 913–920.
59. Sarkar, D. K.; Bera, S.; Dhara, S.; Nair, K. G. M.; Narasimhan, S. V.; Chowdhury, S. XPS Studies on Silicide Formation in Ion Beam Irradiated Au/Si System. *Appl. Surf. Sci.* **1997**, *120*, 159–164.
60. Mason, M. Electronic Structure of Supported Small Metal Clusters. *Phys. Rev. B* **1983**, *27*, 748–762.
61. Peters, S.; Peredkov, S.; Neeb, M.; Eberhardt, W.; Al-Hada, M. Size-Dependent XPS Spectra of Small Supported Au-clusters. *Surf. Sci.* **2013**, *608*, 129–134.
62. Safaei, A. Shape, Structural, and Energetic Effects on the Cohesive Energy and Melting Point of Nanocrystals. *J. Phys. Chem. C* **2010**, *114*, 13482–13496.
63. Buffat, P.; Borel, J. P. Size Effect on Melting Temperature of Gold Particles. *Phys. Rev. A* **1976**, *13*, 2287–2298.
64. Dick, K.; Dhanasekaran, T.; Zhang, Z. Y.; Meisel, D. Size-Dependent Melting of Silica-Encapsulated Gold Nanoparticles. *J. Am. Chem. Soc.* **2002**, *124*, 2312–2317.
65. Tsai, H.; Hu, E.; Perng, K.; Chen, M.; Wu, J.-C.; Chang, Y.-S. Instability of Gold Oxide Au_2O_3. *Surf. Sci.* **2003**, *537*, L447–L450.
66. Maya, L.; Paranthaman, M.; Thundat, T.; Bauer, M. L. Gold Oxide as Precursor to Gold/Silica Nanocomposites. *J. Vac. Sci. Technol., B* **1996**, *14*, 15–21.
67. Campbell, C. T. Bimetallic Surface Chemistry. *Annu. Rev. Phys. Chem.* **1990**, *41*, 775–837.
68. Finazzi, E.; Di Valentin, C.; Pacchioni, G. Nature of Ti Interstitials in Reduced Bulk Anatase and Rutile TiO_2. *J. Phys. Chem. C* **2009**, *113*, 3382–3385.
69. Behafarid, F.; Roldan Cuenya, B. Nano Pinstripes: TiO_2 Nanostripe Formation by Nanoparticle-Mediated Pinning of Step Edges. *J. Phys. Chem. Lett.* **2012**, *3*, 608–612.
70. Tromp, R.; Rubloff, G.; Balk, P.; LeGoues, F.; van Loenen, E. High-Temperature SiO_2 Decomposition at the SiO_2/Si Interface. *Phys. Rev. Lett.* **1985**, *55*, 2332–2335.
71. Naitabdi, A.; Behafarid, F.; Roldan Cuenya, B. Enhanced Thermal Stability and Nanoparticle-Mediated Surface Patterning: Pt/TiO_2(110). *Appl. Phys. Lett.* **2009**, *94*, 083102.